Can Iron-porphyrins behave as Single-molecule Magnets?

Aritra Mukhopadhyaya and Md. Ehesan Ali*

Institute of Nano Science and Technology, Mohali, Punjab 140306, India

E-mail: ehesan.ali@inst.ac.in

Abstract

Spin-bearing metal ions encapsulated by macrocyclic ligands in porphyrin complexes make them an ideal component in molecular spintronic devices where there is scope for the logical manipulation of various magnetic properties of the molecular system. Adding an axial ligand to the planar porphyrin complexes is established to be a very useful route to alter different aspects of the magnetochemistry of the resulting complex. Magnetic anisotropy is a lesser-known avenue in this context. For a series of high-spin pentacoordinate d^5 Fe(III) and d^6 Fe(II) porphyrin complexes with varying axial ligands, the magnetic anisotropy parameters are obtained from the spin Hamiltonian formalism. The d^5 high spin complexes, having a net zero orbital angular momentum, possess an almost isotropic magnetic environment. The small positive zero-field splitting (2-7 cm^{-1}) for these complexes arises due to near proximity of the quartet excited states. This ZFS is found to increase down the group for the halide ligands owing to the decrease of the sextet-quartet energy gap. On the other hand, possessing a triaxial anisotropic magnetic environment, the sign and the magnitude of the ZFS parameters of the d^6 complexes are mostly dependent on the axial ligand itself. Amongst the considered complexes, H_2O and NH_3 exhibit positive ZFS while the Imidazole-based ligands possess a negative sign to the ZFS parameter.

Introduction

The diverse and versatile magneto-chemistry of the spin-bearing iron(II) porphyrins has expanded the scope of these archetypal metal-organic complexes beyond their well-known involvements in various biological processes like oxygen transport, electron transfer reactions, catalysis, etc.[1–5] This class of bio-inspired complexes has already marked its presence as an important component in the fields of catalysis, molecular switches, molecular spintronics, and single molecular devices.[2,6–11] Three closely lying spin multiplets, *viz.* the triplet ($S = 1$), quintet ($S = 2$), and singlet ($S = 0$) states dictate the overall magnetochemical behavior of these complexes. The square planar iron(II) porphyrin as an isolated molecule exhibit a triplet ground state.[12–21] The addition of various ligands to the axial coordination sites of the metal center provides a route to manipulate the magneto-chemistry of the metalloporphyrin complexes.[22–34] The change in the ligand environment by such means triggers an alteration in the fundamental magnetic properties like the spin state of the complex, crystal field splitting, etc. On the other hand, the strong chemisorption of the molecule on the substrate induces a set of modifications to the molecular structure that pave the path for manipulating the magnetic state of the molecule. The interaction between the d-electrons of the magnetic center of the molecule and the substrate often leads to the change in the spin state,[35,36] magnetic coupling with the substrate,[7,8,37] magnetic anisotropy of the molecule,[9,38–40] etc. The multi-orbital nature and the spin–orbit coupling induce an anisotropy to the magnetic state of the molecule.[9,41,42] The intermediate spin species exhibit an easy-plane magnetic anisotropy.[19] Reports have shown that owing to the change in spin state upon deposition to a substrate the molecules exhibit an easy axis anisotropy.[39,40] The iron porphyrin molecule has been found to exhibit an easy axis of magnetization and large spin relaxation time when it is deposited on an Au(111) substrate via an on-surface metalation reaction.[39] Several other porphyrin derivatives are found to possess a sizable amount of the zero-field splitting which in turn leads to slow relaxation of the magnetization in the corresponding complex indicating the single-ion magnetic behavior.[38,43] Spin-bearing molecules with the ability to retain the orientation of the magnetic moment in the absence of the magnetic field are called single-molecule magnets.[44–47]

Thus, the ease of manipulation of various magnetic properties of the iron porphyrin complexes via deposition on various substrates [7–9,35–42,48] or via axial ligation [24,26,27] or via the both [11,41,42,49,50] means makes the penta-coordinated porphyrins ideal candidates for the device applications. To date, several attempts have been made to harness the anisotropic environment exerted by the ligand field into a real-time device application for the iron porphyrin complexes.[9,39–42,51] Hence, it becomes imperative to look into the origin of the magnetic anisotropy for various iron porphyrin complexes. Having a net zero orbital angular momentum, there is no first-order spin-orbit coupling contribution for a $3d^5$ iron(III) ion. A very small contribution from the second-order SOC makes the high spin ($S = 5/2$) iron(III) an almost electronically isotropic species.[43] On the other hand, the iron(III) in its intermediate spin state shows significant negative zero field splitting as well as slow magnetic relaxation.[44,52] It is found in various experimental studies that the high spin penta-coordinated iron(III) porphyrins show significant zero-field splitting (ZFS) varying within the range of 1-10 cm^{-1}.[22,24–26] The most popular explanation of this phenomenon is the near proximity of the low-lying spin states due to the presence of the ligand field.[28,43,53] The iron(II) ($3d^6$) in its high spin ($S = 2$) configuration possesses a large orbital angular momentum which in turn leads to a strong uniaxial magnetic anisotropy and slow magnetic relaxation.[54] Although, a lot of dedicated efforts have been bestowed upon understanding the electronic structure of the ground spin state of the iron porphyrin complexes, a very small portion of the studies are focused on unraveling the nature of magnetic anisotropy of these complexes.

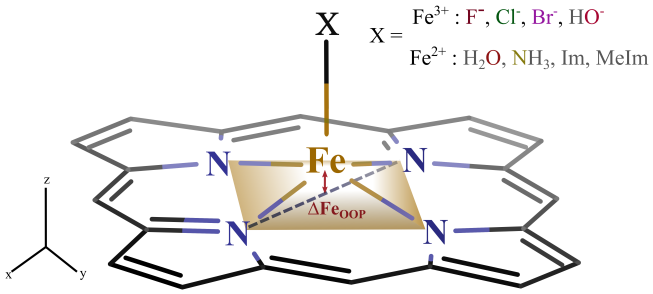

Figure 1: Schematic representation of the penta-coordinated porphyrin complexes. X stands for various axial ligands. The outwards displacement of the porphyrin core is denoted by ΔFe_{OOP}. The blue dotted line represents the imaginary line joining the two opposite nitrogen of the porphyrin macrocycle.

In this work, we have extensively studied the origin and nature of the magnetic anisotropy exhibited by the penta-coordinated iron porphyrin complexes. By considering different atom/group in the axial position (Figure 1), the modification in the ligand field imposed by the axial ligands were studied. We have chosen eight different axial ligands which result in the high spin ground state for the central metal ion iron. On the other hand, the two most common oxidation states; +3 and +2 are considered for the iron atom having d^6 and d^5 electronic systems. For the porphyrin model, we have used the truncated porphine molecule. We have chosen the negatively charged monodentate ligands (F^-, Cl^-, Br^-, OH^-) for the d^5 and neutral monodentate ligands (H_2O, NH_3, Imidazole (Im) and methyl imidazole (MeIm)) for the d^6 systems. Upon carefully investigating the effect of the axial ligation on the structural parameters obtained from hybrid density functionals, we have analyzed the magnetic anisotropy of the considered complexes as obtained from *ab initio* treatment of the ground spin state via CASSCF+NEVPT2 methods. The observed effect of the axial ligands on the nature and magnitude of the magnetic anisotropy parameters of the complexes have been discussed.

Computational details

Spin unrestricted density functional theory (DFT) calculations are performed to obtain the ground state geometry for each complex. The hybrid GGA functional PBE0[55] is used in combination with def2-TZVP[56] basis set. A D3 dispersion correction[57] is included along with a Becke-Johonson damping(D3BJ)[58] for accounting the long-range effects during the geometry optimization cycles. All the molecules are ensured with zero negative vibrational frequencies for all three possible spin states. The adiabatic spin state energies ($\Delta E^{adiabatic}$) with respect to the high spin state are calculated to evaluate the relative spin state energies of the complexes. The vertical spin state energies are also been calculated from DFT-based hybrid functionals as well as a multiconfigurational approach (discussed later).

To understand the effect of the chemical bonding on the magnetic anisotropy parameters, a se-

ries of state-averaged complete active space self-consistent field (SA-CASSCF)[59] methods with N-electron valence second-order perturbation theory (NEVPT2)[60] based calculations are performed using different active spaces. Starting from an active space constructed by distributing the 3*d* electrons in the five Fe 3*d* (CAS(6/5,5)) orbitals. The active space size is denoted as (no of electron for d^6 complex in the active orbitals/same number in case of the d^5 case, no of active orbitals). To account for the nondynamical correlation effects associated with covalency between the iron and the porphyrin macrocycle, a doubly occupied bonding (Fe-N_{Por}) orbital is added resulting in a CAS(8/7,6) space. After adding a second 4*d* (denoted as d') shell to describe the double-shell effect (CAS(6/5,10)), the Peerloot active space (CAS(8/7,11)) for iron porphyrin is constructed which is found to produce the correct ground spin state for the porphyrin complexes.[16,29,31,32,61] The axial ligands studied here can show σ (σ_{Fe-X}) and π ($\pi_{X\rightarrow Fe}$) bonding interactions with the iron center and hence call for extensive understanding of the nature of the bonding interactions for individual ligands. Thus, the molecular orbitals that inherit both the σ and π bonding interactions of the Fe-X chemical bonds, whenever important, are considered in the active space after obtaining a preliminary idea about the nature of the bonding from the DFT results for a particular complex.

Estimation of magnetic anisotropy: The *ab initio* treatment via the spin Hamiltonian approach calculates the zero-field splitting (ZFS) parameters as[62]

$$\hat{H}_{ZFS} = \vec{S} \cdot \overline{\overline{D'}} \cdot \vec{S} \tag{1}$$

where D' is a symmetric 2nd order traceless tensor and hence can be expressed in terms of two constants; D and E as

$$\hat{H}_{ZFS} = D[S_z^2 - \frac{1}{3}S(S+1)] + E[S_x^2 - S_y^2]$$
$$\text{where, } D = \frac{3}{2}D'_{zz},\ E = \frac{1}{2}(D'_{xx} - D'_{yy})$$

D and E are called axial and rhombic ZFS parameters. The D parameterizes the uniaxiality of

the magnetization in the absence of any external magnetic field.

The spin Hamiltonian parameters are obtained by considering both the static and the dynamic correlation via the CASSCF+NEVPT2 methods.[63] The Douglas-Kroll-Hess (DKH) approximation is included in the calculations to account for the scalar relativistic effects. Compatible with the level of theory the DKH-def2-TZVP basis set is used.[64] The contribution of the spin-orbit coupling to the ZFS is calculated from the quasi-degenerate perturbation theory (QDPT) where the SOC operator is obtained from the spin-orbit mean field (SOMF) treatment.[65,66] All the calculations are performed in the ORCA 5.0.3 program package.[67]

Results and discussion

The relative energies of the optimized geometries at different spin states obtained from the PBE0/def2-TZVP level of theory establish the high spin electronic configuration ($S = 5/2$ for d^5 and $S = 2$ for d^6 systems) to be the ground state for all of the complexes. (SI Table S1) The optimized structural

Table 1: Comparison of different optimized structural parameters for high spin states of penta-coordinated iron porphyrin complexes obtained from hybrid-functional calculations at the PBE0/def2-TZVP level.

Molecule	$\mathbf{d_{Fe-N1}}$ **(Å)**	$\mathbf{d_{Fe-N2}}$ **(Å)**	∠**N1FeN2** (°)	$\mathbf{d_{Fe-N3}}$ **(Å)**	$\mathbf{d_{Fe-N4}}$ **(Å)**	∠**N3FeN4** (°)	$\mathbf{d_{Fe-X}}$ **(Å)**	ΔFe_{OOP} **(Å)**
FePorF [a]	2.078	2.078	153.200	2.078	2.078	153.200	1.785	0.482
FePorCl [b]	2.077	2.078	152.503	2.078	2.077	152.502	2.196	0.494
FePorBr [c]	2.074	2.075	153.244	2.074	2.074	153.244	2.355	0.480
FePorOH	2.083	2.087	152.379	2.089	2.087	151.830	1.818	0.498
FePorH20	2.070	2.072	172.280	2.050	2.065	168.776	2.241	0.139
$FePorNH_3$	2.077	2.077	169.060	2.062	2.065	166.518	2.221	0.198
FePorIm [d]	2.079	2.084	167.648	2.068	2.068	163.405	2.153	0.298
FePorMeIm [e]	2.087	2.087	164.055	2.071	2.073	161.982	2.170	0.324

[a] Anzail et al., single crystal[68] d_{Fe-N}: 2.072 Å, $\Delta Fe_{(OOP)}$: 0.47 Å, d_{Fe-Cl}: 1.792 Å.
[b] Scheidt et al., single crystal;[69] d_{Fe-N}: 2.068 Å, $\Delta Fe_{(OOP)}$: 0.49 Å, d_{Fe-Cl}: 2.192 Å.
[c] Behere et al., single crystal;[26] d_{Fe-N}: 2.069 Å, $\Delta Fe_{(OOP)}$: 0.56 Å, d_{Fe-Br}: 2.348 Å.
[d] Ali et al. DFT, B3LYP[15] ; d_{Fe-N}: 2.11 Å, $\Delta Fe_{(OOP)}$: 0.43 Å, $d_{Fe-N(Im)}$: 2.16 Å.
[e] Hu et al., single crystal;[27] ; d_{Fe-N}: 2.08 Å, $\Delta Fe_{(OOP)}$: 0.36 Å, $d_{Fe-N(Im)}$: 2.18 Å.

parameters corroborate nicely with the experimental structure and reveal that the presence of an axial ligand induces a set of major modifications in the molecular geometries as well as in the electronic structures in an iron porphyrin complex. As an immediate effect of the axial ligation, the movement of the iron atom from the porphyrin plane (ΔFe_{OOP} in Table 1) leads to the doming shape of the planar porphyrin core which is quantified by the angle between two opposite iron nitrogen bonds (Figure 1 and $\angle N1FeN2$ and $\angle N3FeN4$ in Table 1). The out-of-plane movement of the iron atom from the porphyrin plane is a very significant quantity that needs to be considered with utmost care. The incorporation of the dispersion correction during the geometry optimization produces structural parameters quite close to the experimentally reported structures. The ΔFe_{OOP} computed in this work is found to be nicely corroborating with their counterparts reported in the experiments. It is noteworthy to mention here that the PBE0+D3+def2-TZVP predicts a smaller ΔFe_{OOP} (0.01-0.08 Å) as compared to the experimental value, while the other structural parameters are in very good agreement. The previous computational report where the dispersion correction is not used predicted a larger ΔFe_{OOP} as compared to the experiment. The axial ligation, for some complexes, incorporates some degree of inequivalence to the in-plane Fe-N bonds. For the halide ligands, all the four Fe−N bond distances are equal. Only the FePorOH shows a very small difference in the Fe−N bond distances among the d^5 complexes. On the contrary, the inequivalence in the in-plane bond distances is more pronounced for the d^6 complexes. The overall reduction in the symmetry of the complex due to he d^5 systems show a larger amount of displacement of the iron atom from the porphyrin core as compared to the d^6 complexes. The increased positive charge on the iron atom in the Fe^{3+} results in a higher electron affinity. This facilitates a stronger bonding of the metal center and the ligands in the corresponding complexes. As a result, the bond orders (Table 2) for both the axial and the equatorial bonds in the d^5 porphyrin complexes become larger as compared to the d^6 complexes. Although the internuclear distance between the metal and the axial ligand (d_{Fe-X} in Table 1) changes significantly the out-of-plane displacement of the iron atom from the porphyrin plane remains almost identical. On the other hand, for the d^6 complexes the ΔFe_{OOP} and $\angle N1FeN3$ vary significantly with the change of the axial ligand while the d_{Fe-X}

remains almost identical. This signifies the non-uniform ligand field exerted by various axial ligands. Throughout the following subsections, upon understanding the ground electronic structure of the penta-coordinated porphyrin complexes we are going to correlate the trends and the nature of their magnetic anisotropy parameters.

The electronic structure of the ground spin state

Table 2: Electronic structure properties obtained from PBE0+def2-TZVP calculation.

Molecule	Mayer bond order(MBO)		Löwdin charge population					
	Fe−N(Por)	Fe−X	d_{xy}	d_{xz}	d_{yz}	d_{z^2}	$d_{x^2-y^2}$	Total
FePorF	0.63	0.87	1.07	1.27	1.27	1.41	1.55	6.57
FePorCl	0.64	1.03	1.07	1.31	1.31	1.53	1.55	6.77
FePorBr	0.65	1.03	1.08	1.30	1.30	1.56	1.55	6.79
FePorOH	0.60	1.03	1.07	1.28	1.32	1.44	1.52	6.63
$FePorH_2O$	0.55	0.24	1.07	1.98	1.13	1.20	1.50	6.89
$FePorNH_3$	0.54	0.29	1.07	1.97	1.12	1.24	1.49	6.90
FePorIm	0.56	0.41	1.07	1.13	1.96	1.25	1.49	6.89
FePorMeIm	0.57	0.40	1.07	1.17	1.93	1.24	1.48	6.89

A. d^5 Iron(III) porphyrins: The residence of the five unpaired electrons in the five d orbitals leads to a high spin ($S = 5/2$) $^6A'$ term for the d^5 complexes. It is noteworthy to mention here that, despite the near identical structural features, slight differences are observed in the bond order of the iron halogen bonds. The chloride and bromide show higher bond order for the Fe-X bond (Table 2). The weak possibility for the π-donation of the non-bonding electrons from the fluoride to the iron center makes the Fe-F bonds weaker as compared to the Fe-Cl or Fe-Br bonds. The later ones exhibit a prominent signature of the π-bonding as observed in an increase in the population at the d_{xz} and d_{yz} orbitals of the iron atom (Table 2). This bonding information turns out to be crucial for choosing the active space for the CASSCF calculations. To account for the effect of the bonding of the axial ligands, on top of the Peerloot CAS (7,11) space, two electrons from the σ bond between the iron atom and the axial ligand (σ_{Fe-X} in Figure S1-S4 in the SI) is included as the active orbitals, resulting in a CAS (9,12) space. Depending upon the extent of the π bonding we have also included the π orbitals between the metal and the axial ligands into the active space.

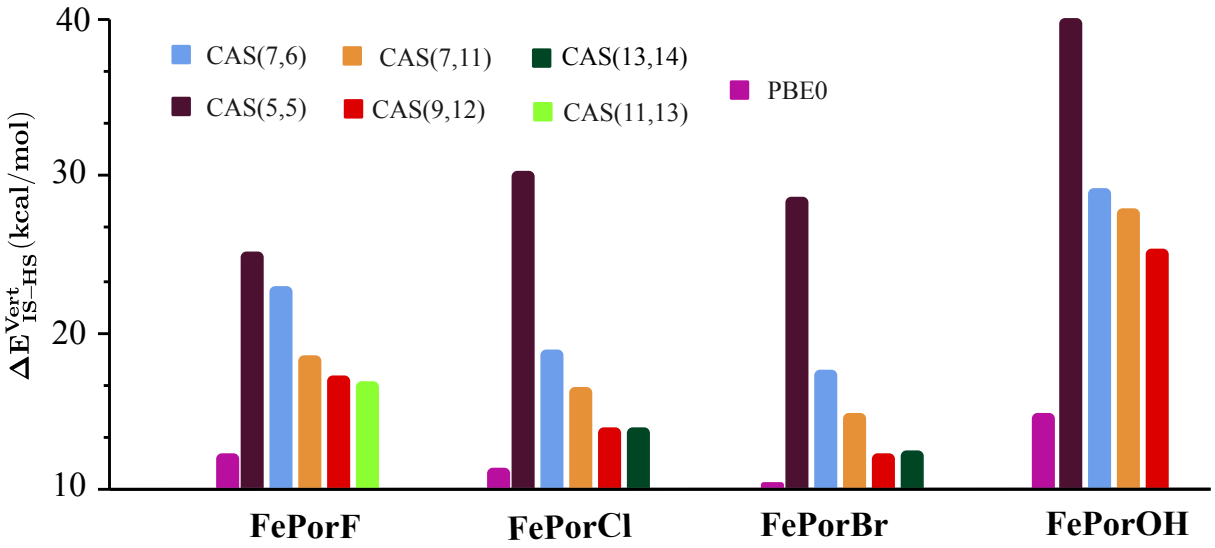

Figure 2: Vertical spin state energies of the d^5 iron(III) porphyrin complexes obtained from different methods.

For FePorF only one π orbital is included in the active space leading to a CAS (11,13) active space (Figure S1). While, for the FePorCl and FePorBr two π orbitals were included in the active space with the rise in the active space size to 13 electrons in 14 orbitals (Figure S2-S3). For FePorOH, the active space is limited to the CAS(9,12) space due to the absence of the π bonding interaction between the metal and the OH^- ligand (Figure S4).

It is imperative to understand the effect of the axial ligands on stabilizing the sextet ground spin state. The closest electronic states to the ground spin state are of lower multiplicity with $S = 3/2$. The vertical spin state energies computed on the relaxed geometry of the high spin state are summarized in Figure 2. The vertical energies computed from the PBE0 hybrid functional account for the difference in the total energies computed with multiplicity 6 and 4 on the ground state optimized geometries for each complex. The E^{Vert} computed from the CASSCF methods represents the energy difference between two lowest-lying electronic states of two different multiplicities after treating the CASSCF converged wavefunctions with second-order perturbation treatment with NEVPT2 formalism. It is found that the minimal active space containing the five unpaired electrons (CAS(5,5)) largely overestimates the spin state energies compared to the other CASSCF spaces (Figure 2). This stabilization of the high spin ground state is reduced with the inclusion

of the σ bonding interactions from porphyrin (CAS(7,6)) as well as the axial ligands. The inclusion of the double d-shell (CAS(7,11)) is also found to be lowering the energy gap. Furthermore, when we have appended the CAS space with the σ_{Fe-X} bond the energy is further reduced with the CAS(9,12) space. Although the addition of the π electrons doesn't further improve the performance of the CAS wavefunction, the largest active space for a molecule described in SI (CAS(11,13) for FePorF, CAS(13,14) for FePorCl and FePorBr and CAS(9,12) for FePorOH) is used to evaluate the magnetic anisotropy parameters. Although the structural changes imposed by the axial ligands are of very minute amount, the obvious trend that can be derived from the vertical spin state energy gaps is $\Delta E_{OH} > \Delta E_F > \Delta E_{Cl} > \Delta E_{Br}$.

B. d^6 **Iron(II) porphyrins:** Addition of one axial ligand (H_2O, NH_3, Im, MeIm) to the axial position to the d^6 iron porphyrin system modifies the ligand environment around the iron atom and results in a change in the spin states of the complexes from intermediate ($S = 1$) to high spin ($S = 2$). The monodentate ligands considered here tend to inherit a similar ligand environment as all of them form the coordinate bond with the iron atom via a lone pair of electrons. Axial ligation of those ligands imparts noticeable out-of-plane displacement of the iron atom from the porphyrin core which can be correlated to a larger Fe-X bond order (MBO in the Table 2). For H_2O and NH_3, the lone pair of electrons resides in an sp^3 hybridized orbital. As we move to the Im and MeIm, the lone pair is accommodated in an sp^2 hybridized orbital which has a smaller size and hence will procure a stronger bonding with the metal center. The identical population at the d_{xz} and d_{yz} orbitals of the metal in FePorIm as compared to the other complexes nullifies the possibility of the additional π bonding between the metal and the axial ligand. However, the orientation of the imidazole ligand facilitates the interaction between the p_z orbital of the N atom and the d_{xz} orbital of the iron atom. This interaction lowers the energy of d_{yz} orbital and makes it doubly occupied. This changes the ground electronic configuration for the FePorIm. Ligation with H_2O and NH_3 results in ${}^5A''(d^2_{xz}, d^1_{yz}, d^1_{z^2}, d^1_{xy}, d^1_{x^2-y^2})$ as the ground state while imidazole (Im) and methyl imidazole (MeIm) produce ${}^5A'(d^2_{yz}, d^1_{xz}, d^1_{z^2}, d^1_{xy}, d^1_{x^2-y^2})$ as the ground state. As the only significant bonding interaction present between the axial ligand and the metal is the σ bonding,

only the orbital from the $Fe-X$ bonding has been appended to the Peerloot's active space resulting in a CAS (10,12) space.

The vertical spin state energies calculated from PBE0/def2-TZVP calculation and the NEVPT2 treated CASSCF wavefunction are compared in the Figure 3. The vertical energy gap calculated with the largest CAS(10,12) space corroborated nicely with the previously reported values by Vancoillie et al.[16] by means of the CASPT2 calculations. Among all the CAS space the CAS(8,6) gives the lowest energy gap after the NEVPT2 treatment. PBE0 underestimates the spin energy gap. The ground electronic configurations depicted by the PBE0 are reproduced by the CASSSCF+NEVPT2 calculations. The relative order of the vertical spin state energies remains the same irrespective of the underlying computational method used. This trend of the vertical spin state energies clearly establishes the influence of the axial ligand on the ground state of the complex.

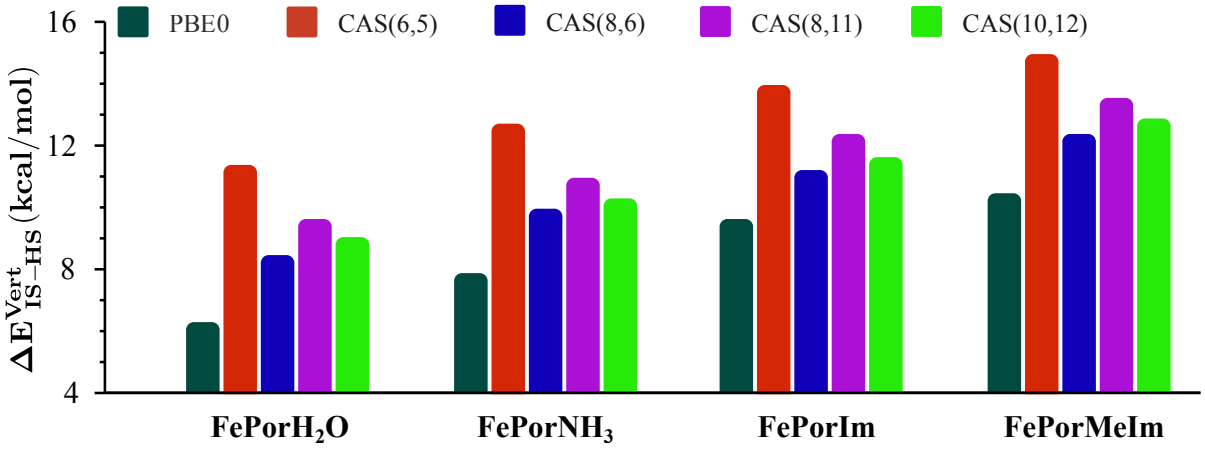

Figure 3: Vertical spin state energies of the d^6 iron(II) porphyrin complexes obtained from different methods.

Effect of axial ligation on the zero-field splitting parameters and magnetic anisotropy

A. d^5 iron(III) porphyrins: The trend of the zero-field splitting parameter D amongst the d^5 pentacoordinated porphyrin complexes is quite controversial. Different experiments reported different trends of the ZFS parameters. Marikondi et al. have reported a higher D for FePorCl than Fe-

Table 3: Comparison of magnetic anisotropy of the penta-coordinated porphyrin complexes as obtained from the CASSCF+NEVPT2 calculations from the effective Hamiltonian formalism.

Molecule	CAS space	D	D^{Exp}	E/D	g_x	g_y	g_z	g_z/g_x	GS*
d^5-System									
FePorF	CAS(11, 13)	3.90	5.5[#]	0.00	1.99	1.99	2.00	1.001	$^6A'$
FePorCl	CAS(13, 14)	4.80	6.46[†]	0.00	2.00	2.00	2.00	1.002	$^6A'$
FePorBr	CAS(13, 14)	6.64	12.5 [◇]	0.00	2.00	2.00	2.00	1.003	$^6A'$
FePorOH	CAS(11, 13)	2.06	-	0.07	2.00	2.00	2.00	1.000	$^6A'$
d^6-System									
$FePorH_2O$	CAS(10, 12)	6.21	-	0.22	2.11	2.17	2.28	1.078	$^5A''$
$FePorNH_3$	CAS(10, 12)	15.58	-	0.02	2.06	2.19	2.35	1.141	$^5A''$
FePorIm	CAS(10, 12)	-11.98	5-30 [‡]	0.02	2.07	2.16	2.30	1.114	$^5A'$
FePorMeIm	CAS(10, 12)	-20.19	5-30 [‡]	0.17	2.02	2.10	2.43	1.21	$^5A'$

[#] Brackett et al.[23] for ferrihemoglobin-F. [†] Nehrkorn et al. for FeTPPCl[34] . [◇] Behere et al.[26] for FeTPPBr. [‡] Hu et al.[27] for Imidazole complexes of FeOEP.
*GS stands for ground state electronic term. The details of the other excited electronic states are given in Figures 5 and 7 and Table S2-S5 and S7-10.

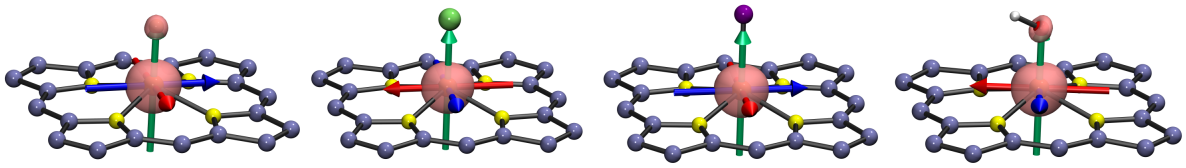

Figure 4: Orientation of the g_x, g_y, and g_z components of the g-tensor (shown by red, blue, and green vectors respectively) with respect to the molecular frame for the d^5 iron porphyrin complexes. The length of the vectors is scaled according to the eigenvalues of the respective g-tensor component. The pink iso-surface represents the distribution of the spin density with an iso-surface value of $0.05\mu_B/\AA^3$. Color code: C-ice-blue, N-yellow, Fe-orange, O-red, F-brown, Cl-lime, Br-purple, H-silver.

PorBr[22] which is later contradicted by Behere et al.[24,26] These contradicting studies are unable to establish the actual effect of the axial ligands in the zero-field splitting in d^5 porphyrin complexes. In Table 3, the parameters determining the nature of the magnetic anisotropy of the d^5 pentacoordinated porphyrin complexes have been reported as obtained from our CASSCF+NEVPT2 calculations. The same parameters obtained from the smaller active spaces are given in the SI. The three identical components of the g-tensor suggest an isotropic magnetic ($g_x = g_y = g_z$) environment at

the magnetic centers for all the d^5 porphyrin complexes. However, a small positive axial zero-field splitting is observed for all the molecules. The orientation of the components of the g-tensor (Figure 4) shows that the main magnetic axis (g_z) is aligned with the principal axis of symmetry that is the bonding axis between the iron and the axial ligand. The other two axes lie in the porphyrin plane and are diagonal to the iron-nitrogen bonds. All the complexes show similar relative orientations of the g-tensor components. The D-values can be ordered as $D_{OH} < D_F < D_{Cl} < D_{Br}$, which is exactly the reverse order of the vertical energy gap between the high spin and intermediate spin states. In other words, the proximity of the intermediate spin state to the high spin state gives rise to a larger positive zero-field splitting parameter in the d^5 porphyrin complexes. As shown in the Figure 5 (Table S2-S5), the major zero field anisotropy is arising due to the excited quartet state ($^4A''$). The established trend of the D remains unaltered irrespective of the size of the active orbitals (Table S6). The near proximity of the quartet excited state also induces a spin state mixing in the ground state which is reflected in the composition of the ground state electronic wave function (Table S2-S5).

B. d^6 iron(II) porphyrins: As reported by Tarrago and co-workers from their combined experimental and theoretical study, the iron(II) tetraphenyl porphyrin complex in intermediate spin state is found to exhibit an easy plane magnetic anisotropy ($g_{\parallel} < g_{\perp}$) with a large positive zero field parameter of $\sim 94\ cm^{-1}$.[19] Owing to the change in the spin state and the electronic structure in the penta-coordinated square pyramidal porphyrins, the magnetic anisotropy is also changed. Three non-uniform values of the g-tensor components ($g_x < g_y < g_z$) suggest a triaxiality of the magnetic anisotropy in the considered complexes.[70,71] The orientation of the main magnetic axis changes according to the nature of the axial ligand (Figure 6). For the H_2O and NH_3, the main magnetic axis is nearly collinear with the bonding axis between the iron and the axial ligand. The other two components of the g-tensor lie near the iron-nitrogen bonds on the porphyrin plane. For the Im and the MeIm, the main magnetic axis (g_z) deviates from the principal axis and lines up with the iron nitrogen bond. On the other hand, the g_y components of the corresponding complexes are collinear with the axial ligand. The H_2O and NH_3 induce a small positive zero-field splitting parameter

while Im and MeIm give rise to a comparatively large negative ZFS. Several imidazole complexes have been studied earlier by Hu and co-workers[27] and resulted in an inconclusive sign of the ZFS parameter. However, the consistent negative sign of the ZFS over a large number of active spaces for both the imidazole complexes in our calculations unequivocally establishes the negative sign of the ZFS for those complexes. Unlike the d^5 complexes, the first two excited electronic states of the d^6 complexes are also quintet states. As shown in Figure 7, the excitations that give rise to the ZFS are the excitation from the ground quintet state to the first excited quintet state. As discussed earlier, the ground electronic term also depends upon the axial ligand. A smaller energy gap between the ground quintet state and the first excited quintet state results in a larger D-value and hence D is unrelated to the quintet-to-triplet energy gap.

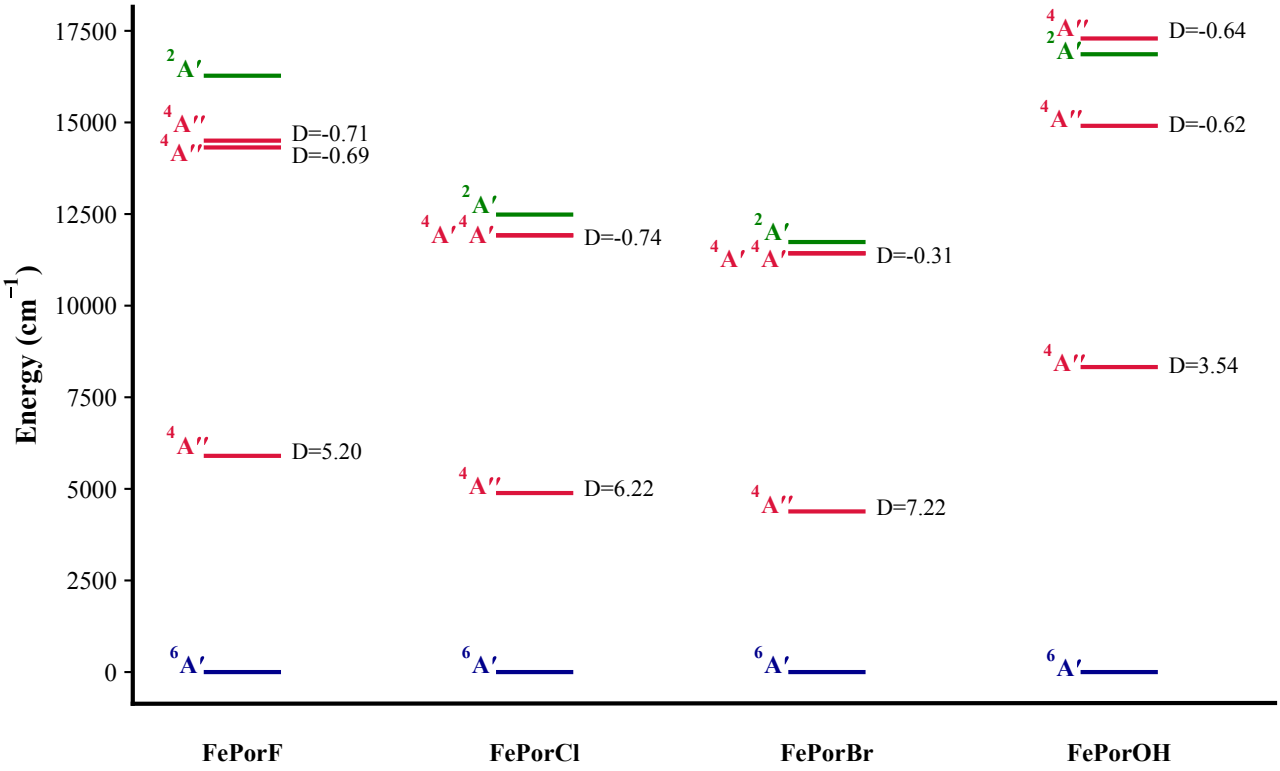

Figure 5: Relative ordering of the electronic configurations as obtained from CASSCF+NEVPT2 calculations for the d^5 complexes studied here. The molecular term corresponding to a particular electronic configuration is placed above the energy level. The values corresponding to D represent the contribution of that particular electronic configuration towards the total ZFS parameter D in cm^{-1} unit. Only those configurations are shown here that contribute more than ± 0.5 cm^{-1}.

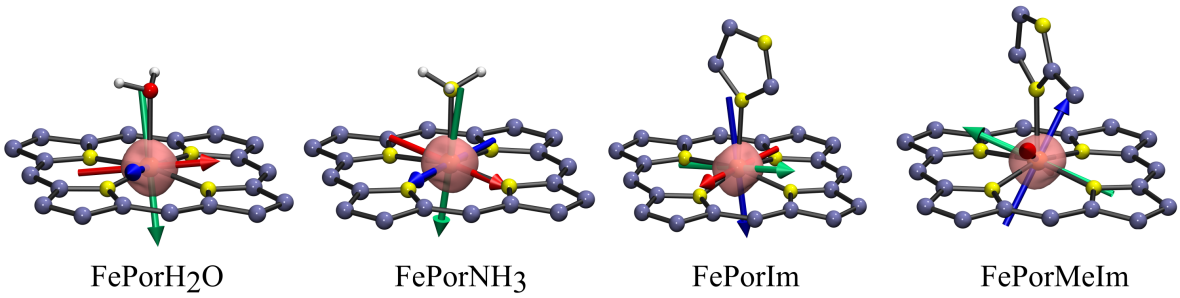

Figure 6: Orientation of the g_x, g_y, and g_z components of the g-tensor (shown by red, blue, and green vectors respectively) with respect to the molecular frame for the d^5 iron porphyrin complexes. The length of the vectors is scaled according to the eigenvalues of the respective g-tensor component. The pink iso-surface represents the distribution of the spin density with an iso-surface value of $0.05\mu_B/\AA^3$. The same color code as Figure 4 is used here.

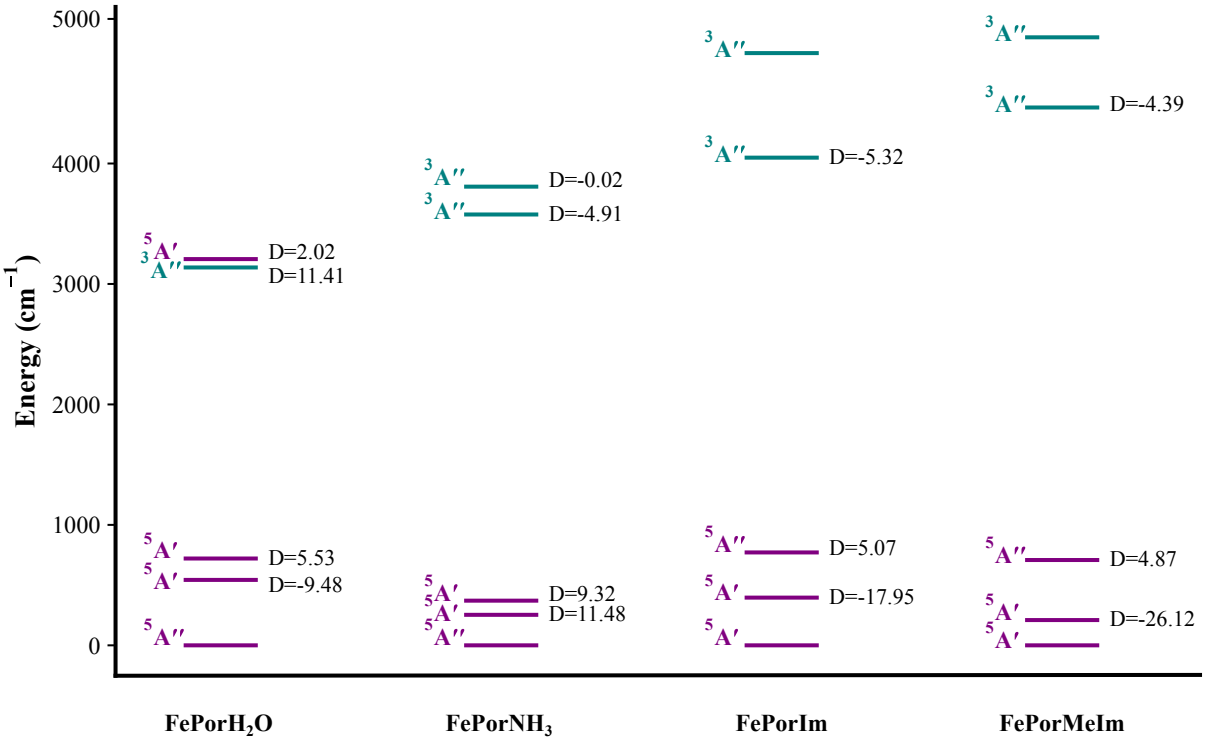

Figure 7: Relative ordering of the electronic configurations as obtained from CASSCF+NEVPT2 calculations for the d^6 complexes studied here. The molecular term corresponding to a particular electronic configuration is placed above the energy level. The values corresponding to D represent the contribution of that particular electronic configuration towards the total ZFS parameter D in cm^{-1} unit. Only those configurations are shown here which contribute more than ± 0.5 cm^{-1}.

Conclusions

Within a series of the penta-coordinated high spin iron(II/III) porphyrin complexes, the structural distortion to the planar porphyrin core inserted by the axial ligands is dependent on the ligand itself as well as on the oxidation state of the metal. The out-of-plane movement of the iron atoms in the d^5 iron(III) porphyrin is less pronounced compared to the d^6 iron(II) porphyrins. For the iron(III) halides, the small positive value of the D parameter is attributed to the proximity of the excited quartet state to the ground sextet state. The order of the D parameter for these complexes is $D_F < D_{Cl} < D_{Br}$ which follows the inverse trend of the vertical spin state energy gap between the sextet and the quartet states. On the other hand, the d^6 iron(II) porphyrins show a triaxial kind of anisotropy with $g_x < g_y < g_z$ which in turn is significantly influenced by the axial ligands. The zero-field splitting in these complexes arises due to the transitions between the nearly degenerate quintet states. While the proximity of the first excited quintet regulates the value of the ZFS parameter, the sign of the ZFS depends upon the nature of the bonding between the iron and the axial ligand itself. The H_2O and NH_3 give rise to a small positive ZFS parameter while the imidazole-based ligands result in a significantly negative ZFS for the corresponding complexes. Thus, the axial ligation to the iron center in the iron(II/III) porphyrin complex can significantly influence the nature as well as the magnitude of the zero field splitting and hence can be very crucial in designing the porphyrin-based single molecular magnets.

Acknowledgement

Financial support from the Department of Science and Technology (DST) through the SERB-CRG project No. CRG/2019/003237 and CRG/2022/008683 is gratefully acknowledged. Ms. Sakshi Nain is greatly acknowledged for useful scientific discussions.

Supporting Information Available

Active orbitals with population, the composition of the electronic states included in the CASSCF calculation, and results from smaller CASSCF space.

Conflict of interests

There is no conflict of interest to declare.

References

(1) Kadish, K.; Smith, K. M.; Guilard, R. *The porphyrin handbook*; Elsevier, 2000; Vol. 3.

(2) Gottfried, J. M. Surface chemistry of porphyrins and phthalocyanines. *Surf. Sci. Rep.* **2015**, *70*, 259–379.

(3) Auwärter, W.; Écija, D.; Klappenberger, F.; Barth, J. V. Porphyrins at interfaces. *Nat. Chem.* **2015**, *7*, 105–120.

(4) Kumar, A. Advances in tetrapyrrole complexes spin interfaces. *Materials Today: Proceedings* **2020**, *37*, 2858–2863.

(5) Kingsbury, C. J.; Senge, M. O. The shape of porphyrins. *Coord. Chem. Rev.* **2021**, *431*, 213760.

(6) Wende, H. et al. Substrate-induced magnetic ordering and switching of iron porphyrin molecules. *Nat. Mater* **2007**, *6*, 516–520.

(7) Bernien, M.; Miguel, J.; Weis, C.; Ali, M. E.; Kurde, J.; Krumme, B.; Panchmatia, P. M.; Sanyal, B.; Piantek, M.; Srivastava, P., et al. Tailoring the nature of magnetic coupling of Fe-porphyrin molecules to ferromagnetic substrates. *Phys. Rev. Lett.* **2009**, *102*, 047202.

(8) Girovsky, J. et al. Long-range ferrimagnetic order in a two-dimensional supramolecular Kondo lattice. *Nat. Commun.* **2017**, *8*, 15388.

(9) Yang, K.; Chen, H.; Pope, T.; Hu, Y.; Liu, L.; Wang, D.; Tao, L.; Xiao, W.; Fei, X.; Zhang, Y. Y.; Luo, H. G.; Du, S.; Xiang, T.; Hofer, W. A.; Gao, H. J. Tunable giant magnetoresistance in a single-molecule junction. *Nat. Commun.* **2019**, *10*, 1–7.

(10) Rubio-Verdú, C.; Sarasola, A.; Choi, D. J.; Majzik, Z.; Ebeling, R.; Calvo, M. R.; Ugeda, M. M.; Garcia-Lekue, A.; Sánchez-Portal, D.; Pascual, J. I. Orbital-selective spin excitation of a magnetic porphyrin. *Commun. Phys.* **2018**, *1*, 1–7.

(11) Vaxevani, K.; Li, J.; Trivini, S.; Ortuzar, J.; Longo, D.; Wang, D.; Pascual, J. I. Extending the Spin Excitation Lifetime of a Magnetic Molecule on a Proximitized Superconductor. *Nano Lett.* **2022**, *22*, 6075–6082.

(12) Kitagawa, T.; Teraoka, J. The resonance Raman spectra of intermediate-spin ferrous porphyrin. *Chem. Phys. Lett.* **1979**, *63*, 443–446.

(13) Abe, M.; Kitagawa, T.; Kyogoku, Y. Resonance Raman spectra of octaethylporphyrinato-Ni(II) and meso-deuterated and 15N substituted derivatives. II. A normal coordinate analysis. *J. Chem. Phys.* **1978**, *69*, 4526–4534.

(14) Ghosh, A. Electronic structure of corrole derivatives: insights from molecular structures, spectroscopy, electrochemistry, and quantum chemical calculations. *Chem. Rev.* **2017**, *117*, 3798–3881.

(15) Ali, M. E.; Sanyal, B.; Oppeneer, P. M. Electronic structure, spin-states, and spin-crossover reaction of heme-related Fe-porphyrins: A theoretical perspective. *J. Phys. Chem. B* **2012**, *116*, 5849–5859.

(16) Vancoillie, S.; Zhao, H.; Radoń, M.; Pierloot, K. Performance of CASPT2 and DFT for relative spin-state energetics of heme models. *J. Chem. Theory Comput.* **2010**, *6*, 576–582.

(17) Li Manni, G.; Alavi, A. Understanding the Mechanism Stabilizing Intermediate Spin States in Fe(II)-Porphyrin. *J. Phys. Chem. A* **2018**, *122*, 4935–4947.

(18) Li Manni, G.; Kats, D.; Tew, D. P.; Alavi, A. Role of Valence and Semicore Electron Correlation on Spin Gaps in Fe(II)-Porphyrins. *J. Chem. Theory Comput.* **2019**, *15*, 1492–1497.

(19) Tarrago, M.; Römelt, C.; Nehrkorn, J.; Schnegg, A.; Neese, F.; Bill, E.; Ye, S. Experimental and Theoretical Evidence for an Unusual Almost Triply Degenerate Electronic Ground State of Ferrous Tetraphenylporphyrin. *Inorg. Chem.* **2021**, *60*, 4966–4985.

(20) Roemelt, M.; Pantazis, D. A. Multireference approaches to spin-state energetics of transition metal complexes utilizing the density matrix renormalization group. *Adv. Theory Simul.* **2019**, *2*, 1800201.

(21) Mukhopadhyaya, A.; Sharma, M.; Oppeneer, P. M.; Ali, M. E. Probing the spin states of tetra-coordinated iron (II) porphyrins by their vibrational and pre K-edge x-ray absorption spectra. *Int. J. Quantum Chem.* **2023**, *123*, e27174.

(22) Maricondi, C.; Swift, W.; Straub, D. K. Thermomagnetic analysis of hemin and related compounds. *J. Am. Chem. Soc.* **1969**, *91*, 5205–5210.

(23) Brackett, G. C.; Richards, P.; Caughey, W. Far-infrared magnetic resonance in Fe (III) and Mn (III) porphyrins, myoglobin, hemoglobin, ferrichrome A, and Fe (III) dithiocarbamates. *J. Chem. Phys.* **1971**, *54*, 4383–4401.

(24) Behere, D. V.; Marathe, V. R.; Mitra, S. Paramagnetic anisotropy and zero-field splitting in tetraphenylporphinatoiron(III) chloride. *J. Am. Chem. Soc.* **1977**, *99*, 4149–4150.

(25) Behere, D.; Date, S.; Mitra, S. Magnetic susceptibility, anisotropy, low temperature magnetisation and zero field splitting in tetraphenylporphynato iron(III) bromide. *Chem. Phys. Lett.* **1979**, *68*, 544–548.

(26) Behere, D. V.; Birdy, R.; Mitra, S. Effect of Axial Interaction in High-Spin Iron(III) Porphyrins. Paramagnetic Anisotropy and Zero-Field Splitting in (Tetraphenylporphyrin)iron(III) Thiocyanate and Iodide. *Inorg. Chem.* **1981**, *20*, 2786–2789.

(27) Hu, C.; Roth, A.; Ellison, M. K.; An, J.; Ellis, C. M.; Schulz, C. E.; Scheidt, W. R. Electronic configuration assignment and the importance of low-lying excited states in high-spin imidazole-ligated iron(II) porphyrinates. *J. Am. Chem. Soc.* **2005**, *127*, 5675–5688.

(28) Hu, C.; An, J.; Noll, B. C.; Schulz, C. E.; Scheidt, W. R. Electronic configuration of high-spin imidazole-ligated iron (II) octaethylporphyrinates. *Inorg. Chem.* **2006**, *45*, 4177–4185.

(29) Radon, M.; Pierloot, K. Binding of CO, NO, and O2 to heme by density functional and multireference ab initio calculations. *J. Phys. Chem. A* **2008**, *112*, 11824–11832.

(30) Radon, M. Spin-state energetics of heme-related models from DFT and coupled cluster calculations. *J. Chem. Theory Comput.* **2014**, *10*, 2306–2321.

(31) Phung, Q. M.; Wouters, S.; Pierloot, K. Cumulant Approximated Second-Order Perturbation Theory Based on the Density Matrix Renormalization Group for Transition Metal Complexes: A Benchmark Study. *J. Chem. Theory Comput.* **2016**, *12*, 4352–4361.

(32) Pierloot, K.; Phung, Q. M.; Domingo, A. Spin State Energetics in First-Row Transition Metal Complexes: Contribution of (3s3p) Correlation and Its Description by Second-Order Perturbation Theory. *J. Chem. Theory Comput.* **2017**, *13*, 537–553.

(33) Yamane, T. et al. Analyses of sizable ZFS and magnetic tensors of high spin metallocomplexes. *Phys. Chem. Chem. Phys.* **2017**, *19*, 24769–24791.

(34) Nehrkorn, J.; Bonke, S. A.; Aliabadi, A.; Schwalbe, M.; Schnegg, A. Examination of the Magneto-Structural Effects of Hangman Groups on Ferric Porphyrins by EPR. *Inorg. Chem.* **2019**, *58*, 14228–14237.

(35) Lach, S.; Altenhof, A.; Tarafder, K.; Schmitt, F.; Ali, M. E.; Vogel, M.; Sauther, J.; Oppeneer, P. M.; Ziegler, C. Metal-organic hybrid interface states of a ferromagnet/organic semiconductor hybrid junction as basis for engineering spin injection in organic spintronics. *Adv. Funct. Mater.* **2012**, *22*, 989–997.

(36) Bhandary, S.; Brena, B.; Panchmatia, P. M.; Brumboiu, I.; Bernien, M.; Weis, C.; Krumme, B.; Etz, C.; Kuch, W.; Wende, H., et al. Manipulation of spin state of iron porphyrin by chemisorption on magnetic substrates. *Phys. Rev. B* **2013**, *88*, 024401.

(37) Avvisati, G.; Cardoso, C.; Varsano, D.; Ferretti, A.; Gargiani, P.; Betti, M. G. Ferromagnetic and antiferromagnetic coupling of spin molecular interfaces with high thermal stability. *Nano Lett.* **2018**, *18*, 2268–2273.

(38) Hu, J.; Wu, R. Control of the Magnetism and Magnetic Anisotropy of a Single-Molecule Magnet with an Electric Field. *Phys. Rev. Lett.* **2013**, *110*, 097202.

(39) Liu, B.; Fu, H.; Guan, J.; Shao, B.; Meng, S.; Guo, J.; Wang, W. An Iron-Porphyrin Complex with Large Easy-Axis Magnetic Anisotropy on Metal Substrate. *ACS Nano* **2017**, *11*, 11402–11408.

(40) Meng, X.; Möller, J.; Mansouri, M.; Sánchez-Portal, D.; Garcia-Lekue, A.; Weismann, A.; Li, C.; Herges, R.; Berndt, R. Controlling the Spin States of FeTBrPP on Au(111). *ACS Nano* **2022**,

(41) Heinrich, B. W.; Braun, L.; Pascual, J. I.; Franke, K. J. Protection of excited spin states by a superconducting energy gap. *Nat. Phys.* **2013**, *9*, 765–768.

(42) Heinrich, B. W.; Braun, L.; Pascual, J. I.; Franke, K. J. Tuning the Magnetic Anisotropy of Single Molecules. *Nano Lett.* **2015**, *15*, 4024–4028.

(43) Viciano-Chumillas, M.; Blondin, G.; Clémancey, M.; Krzystek, J.; Ozerov, M.; Armentano, D.; Schnegg, A.; Lohmiller, T.; Telser, J.; Lloret, F., et al. Single-Ion Magnetic Be-

haviour in an Iron (III) Porphyrin Complex: A Dichotomy Between High Spin and 5/2–3/2 Spin Admixture. *Chem. Eur. J.* **2020**, *26*, 14242–14251.

(44) Khurana, R.; Gupta, S.; Ali, M. E. First-principles investigations of magnetic anisotropy and spin-crossover behavior of Fe (III)–TBP complexes. *J. Phys. Chem. A* **2021**, *125*, 2197–2207.

(45) Nain, S.; Khurana, R.; Ali, M. E. Harnessing Colossal Magnetic Anisotropy in Sandwiched 3d2-Metallocenes. *J. Phys. Chem. A* **2022**, *126*, 2811–2817.

(46) Gatteschi, D.; Sessoli, R.; Villain, J. *Molecular Nanomagnets*; Oxford University Press: Oxford, U.K., 2006; Vol. 5.

(47) Sessoli, R. Magnetic molecules back in the race. *Nature* **2017**, *548*, 400–401.

(48) Arruda, L. M.; Ali, M. E.; Bernien, M.; Hatter, N.; Nickel, F.; Kipgen, L.; Hermanns, C. F.; Bißwanger, T.; Loche, P.; Heinrich, B. W., et al. Surface-orientation-and ligand-dependent quenching of the spin magnetic moment of Co porphyrins adsorbed on Cu substrates. *Phys. Chem. Chem. Phys.* **2020**, *22*, 12688–12696.

(49) Ballav, N.; Wäckerlin, C.; Siewert, D.; Oppeneer, P. M.; Jung, T. A. Emergence of on-surface magnetochemistry. *J. Phys. Chem. Lett.* **2013**, *4*, 2303–2311.

(50) Rolf, D.; Lotze, C.; Czekelius, C.; Heinrich, B. W.; Franke, K. J. Visualizing Intramolecular Distortions as the Origin of Transverse Magnetic Anisotropy. *J. Phys. Chem. Lett.* **2018**, *9*, 6563–6567.

(51) Rubio-Verdú, C.; Sarasola, A.; Choi, D.-J.; Majzik, Z.; Ebeling, R.; Calvo, M. R.; Ugeda, M. M.; Garcia-Lekue, A.; Sánchez-Portal, D.; Pascual, J. I. Orbital-selective spin excitation of a magnetic porphyrin. *Comms. Phys.* **2018**, *1*, 1–7.

(52) Feng, X.; Hwang, S. J.; Liu, J.-L.; Chen, Y.-C.; Tong, M.-L.; Nocera, D. G. Slow magnetic relaxation in intermediate spin S= 3/2 mononuclear Fe (III) complexes. *J. Am. Chem. Soc.* **2017**, *139*, 16474–16477.

(53) Nishio, T.; Yokoyama, S.; Sato, K.; Shiomi, D.; Ichimura, A.; Lin, W.; Dolphin, D.; McDowell, C.; Takui, T. Ground-state high-spin iron (III) octaethylporphyrin as studied by single-crystal cw/pulsed ESR spectroscopy. *Synthetic metals* **2001**, *1*, 1820–1821.

(54) Freedman, D. E.; Harman, W. H.; Harris, T. D.; Long, G. J.; Chang, C. J.; Long, J. R. Slow magnetic relaxation in a high-spin iron (II) complex. *J. Am. Chem. Soc.* **2010**, *132*, 1224–1225.

(55) Perdew, J. P.; Burke, K.; Ernzerhof, M. Generalized gradient approximation made simple. *Phys. Rev. Lett.* **1996**, *77*, 3865.

(56) Weigend, F. Accurate Coulomb-fitting basis sets for H to Rn. *Phys. Chem. Chem. Phys.* **2006**, *8*, 1057–1065.

(57) Grimme, S. Semiempirical GGA-type density functional constructed with a long-range dispersion correction. *J. Comput. Chem.* **2006**, *27*, 1787–1799.

(58) Grimme, S.; Ehrlich, S.; Goerigk, L. Effect of the damping function in dispersion corrected density functional theory. *J. Comput. Chem.* **2011**, *32*, 1456–1465.

(59) Olsen, S. Canonical-ensemble state-averaged complete active space self-consistent field (SA-CASSCF) strategy for problems with more diabatic than adiabatic states: Charge-bond resonance in monomethine cyanines. *J. Chem. Phys.* **2015**, *142*.

(60) Angeli, C.; Cimiraglia, R.; Evangelisti, S.; Leininger, T.; Malrieu, J.-P. Introduction of n-electron valence states for multireference perturbation theory. *J. Chem. Phys.* **2001**, *114*, 10252–10264.

(61) Vancoillie, S.; Zhao, H.; Tran, V. T.; Hendrickx, M. F. A.; Pierloot, K. Multiconfigurational second-order perturbation theory restricted active space (RASPT2) studies on mononuclear first-row transition-metal systems. *J. Chem. Theory Comput.* **2011**, *7*, 3961–3977.

(62) Boča, R. Zero-field splitting in metal complexes. *Coord. Chem. Rev.* **2004**, *248*, 757–815.

(63) Maurice, R.; Bastardis, R.; Graaf, C. d.; Suaud, N.; Mallah, T.; Guihery, N. Universal theoretical approach to extract anisotropic spin hamiltonians. *J. Chem. Theory Comput.* **2009**, *5*, 2977–2984.

(64) Pantazis, D. A.; Chen, X.-Y.; Landis, C. R.; Neese, F. All-electron scalar relativistic basis sets for third-row transition metal atoms. *J. Chem. Theory Comput.* **2008**, *4*, 908–919.

(65) Heß, B. A.; Marian, C. M.; Wahlgren, U.; Gropen, O. A mean-field spin-orbit method applicable to correlated wavefunctions. *Chem. Phys. Lett.* **1996**, *251*, 365–371.

(66) Ganyushin, D.; Neese, F. First-principles calculations of zero-field splitting parameters. *J. Chem. Phys.* **2006**, *125*.

(67) Neese, F.; Wennmohs, F.; Becker, U.; Riplinger, C. The ORCA quantum chemistry program package. *J. Chem. Phys.* **2020**, *152*, 224108.

(68) Anzai, K.; Hatano, K.; Lee, Y. J.; Scheidt, W. R. Preparation and molecular stereochemistry of fluoro (meso-tetraphenylporphinato) iron (III). *Inorg. Chem.* **1981**, *20*, 2337–2339.

(69) Scheidt, W. R.; Finnegan, M. G. Structure of monoclinic chloro (meso-tetraphenylporphyrinato) iron (III). *Acta Crystallogr. C Struct. Chem.* **1989**, *45*, 1214–1216.

(70) Novitchi, G.; Jiang, S.; Shova, S.; Rida, F.; Hlavička, I.; Orlita, M.; Wernsdorfer, W.; Hamze, R.; Martins, C.; Suaud, N.; Guihéry, N.; Barra, A. L.; Train, C. From Positive to Negative Zero-Field Splitting in a Series of Strongly Magnetically Anisotropic Mononuclear Metal Complexes. *Inorg. Chem.* **2017**, *56*, 14809–14822.

(71) Damgaard-Møller, E.; Krause, L.; Lassen, H.; Malaspina, L. A.; Grabowsky, S.; Bamberger, H.; McGuire, J.; Miras, H. N.; Sproules, S.; Overgaard, J. Investigating complex magnetic anisotropy in a Co (II) molecular compound: A charge density and correlated ab initio electronic structure study. *Inorg. Chem.* **2020**, *59*, 13190–13200.